

Contents lists available at ScienceDirect

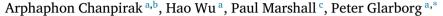
Fuel

journal homepage: www.elsevier.com/locate/fuel



Full length article

An experimental, theoretical, and kinetic modeling study of gas-phase sulfation of KCl



- ^a DTU Chemical Engineering, Technical University of Denmark, DK 2800, Lyngby, Denmark
- ^b Department of Industrial Engineering, Faculty of Engineering, Naresuan University, Phitsanulok 65000, Thailand
- c Department of Chemistry and Center for Advanced Scientific Computing and Modeling, University of North Texas, Denton, TX, USA

ARTICLE INFO

Keywords: KCl sulfation Kinetic modeling Flow reactor

ABSTRACT

The effect of a radical pool on KCl sulfation by SO_2 is investigated through flow reactor experiments on KCl sulfation with and without the presence of CO. These experiments, together with results reported in literature, are interpreted in terms of an updated chemical kinetic model for sulfation. In the absence of combustibles, the rate limiting step in the sulfation of KCl is the oxidation of potassium sulfite to potassium sulfate through the reaction KHSO $_3$ + O $_2$ \rightarrow KHSO $_4$ + O (R17b). Based on chemical kinetic modeling of a range of sulfation experiments, the rate constant for the reverse, exothermic step KHSO $_4$ + O is estimated to be $k_{17} \sim 2 \cdot 10^{12}$ cm 3 mol $^{-1}$ s $^{-1}$. Oxidation of combustibles such as CO facilitates establishment of a radical pool that strongly promotes sulfation. In this case, the sulfation rate is controlled by the oxidation of SO $_2$ to SO $_3$, mostly through SO $_2$ + O (+M) \rightarrow SO $_3$ (+M). An alternative sulfation pathway involving KSO $_4$ as an intermediate is discarded, because the formation through either KO $_2$ + SO $_2$ or KSO $_3$ + O $_2$ involves significant barriers to reaction.

1. Introduction

Inorganic chemistry has important implications for thermal conversion of biomass. During pyrolysis and combustion of biomass at temperatures above about 1073 K, the alkali metals in the fuel (mostly potassium) are partly released to the gas-phase [1-7], typically as alkali chlorides. For agricultural residues, the KCl release can be significant [2,3,7], while woody biomass contains smaller quantities of K and Cl [5,6,8]. Once released, gaseous KCl may cause formation of deposits, corrosion of superheater materials, and emissions of submicron particles and harmful gases [9-11]. Potassium chloride condenses on particulates and heat transfer surfaces during cooling [12-15] or forms an aerosol by homogeneous nucleation [13,14]. In deposits, KCl acts to lower the melting temperature, forming a sticky surface that promotes further deposition [15,16]. Furthermore, its presence in the deposits may lead to severe corrosion by a mechanism where both potassium and chlorine are active in destroying the metal oxide protective layer [17].

The alkali partitioning in combustion of pulverized biomass has been studied in entrained flow reactors [18–20]. Compared to alkali chlorides, alkali sulfates are much less corrosive in deposits [21]. A partial sulfation of alkali chlorides and hydroxides is thus desirable to reduce corrosion. Gaseous KCl may be sulfated by reaction with

 SO_2 and SO_3 [13,14,18,22–31]. Particularly SO_3 is effective and homogeneous sulfation can be promoted by injection of additives that decomposes to SO_3 , i.e., various sulfates [32–34] and sulfuric acid [35]. The reaction between condensed phase KCl and SO_2 is too slow to affect significantly in-flight sulfation [36], but may occur at longer time scales in the deposits [37].

To facilitate design of biomass boilers with a low propensity of deposition and corrosion, it is important to develop reliable models for the fate of the alkali metals, once released to the gas phase [38-41]. A number of studies have reported results for the gas-phase sulfation of KCl [14,23,27-29,31], while data for KOH sulfation are scarce [28]. Glarborg and Marshall [24] proposed a detailed chemical kinetic model for the gas phase sulfation of KCl, in which the oxidation of SO2 to SO₃ was the rate-limiting step, followed by the fast sequence KCl + SO_3 (+M) \rightarrow KClSO₃ (+M), KClSO₃ + H₂O \rightarrow KHSO₄ + HCl, KHSO₄ + KCl \rightarrow K₂SO₄ + HCl. This mechanism has been refined over the years, including additional sulfation steps that do not involve SO₃ and updating of rate constants for key reactions [26-28,30]. Modeling predictions have been shown to be at least qualitatively consistent with sulfation rates for KCl observed in entrained flow reactors [23] and under post-flame conditions [27–29,31,42]. Also, sulfation of KCl by SO₃ is captured satisfactorily [35]. However, a recent flow reactor study of the chemical coupling between CO oxidation and potassium

https://doi.org/10.1016/j.fuel.2024.130974

^{*} Corresponding author.

E-mail address: pgl@kt.dtu.dk (P. Glarborg).

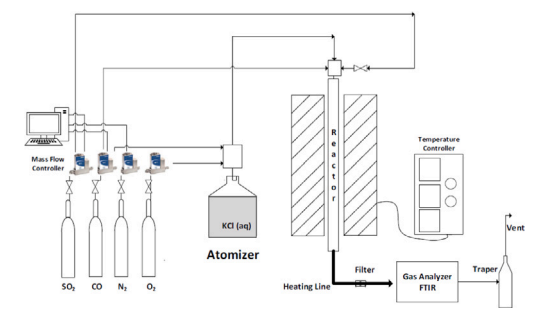


Fig. 1. Schematic of the flow reactor setup.

transformation [43] indicates that KCl sulfation in the presence of combustibles is strongly overpredicted by the model. Since the SO_2/SO_3 interconversion is well established [26,44], the shortcomings of the model are most likely related to reactions of KO_x , KSO_x , and $KHSO_x$ (x = 2-4).

The objective of the present work is to resolve these discrepancies and provide a reliable reaction mechanism for sulfation of KCl through a combined experimental, theoretical, and kinetic modeling study. We examine the effect of the radical pool on KCl sulfation by SO_2 by conducting flow reactor experiments on KCl sulfation with and without the presence of CO. Selected reactions in the alkali subset are analyzed theoretically and the reaction mechanism is updated accordingly. The revised model is developed and validated using both the present experimental results and data reported in literature.

2. Experimental

The experimental setup is described in more detail elsewhere [35, 43,45], and only a brief introduction is provided here. The flow reactor setup, shown in Fig. 1, consisted of a gas dosing system, an electrically heated flow reactor, a filter, a gas-product analysis unit, a gas manometer, and a cooling trap. A total gas flow rate of 2 l/min (298 K, 1 atm) was used in all experiments. Gases with 99.995% purity were supplied from gas cylinders through a particulate filter and a series of precise mass flow controllers.

An atomizer (Model 3076, TSI Inc. Particle Instruments) was used to generate an aerosol from a KCl solution. The solution was prepared from KCl powder (≥99.9%, Sigma-Aldrich Corp.) and deionized water. The atomizer produced a stable aerosol feeding [43]. The gaseous reactants (CO, O2, and H2O in N2) and aerosol flows were mixed in a vessel above the main reactor. The tubular reactor, made of quartz with an inner diameter of 6 mm, was placed in a temperature-controlled electrically heated oven. The length of the isothermal section (± 10 K) was approximately 400 mm. With the chosen flow, this reactor dimension secures a good approximation to plug-flow in the laminar flow regime. The gas flow rate results in a residence time in the isothermal zone of 92/T(K). A quartz filter downstream of the main reactor was used to collect the fine particles. The product gas line and the filter were maintained at 453 K by a heating element cable to avoid the condensation of water and sulfur-containing compounds. The concentrations of CO, CO₂, SO₂, HCl, and H₂O in the exit gas were monitored by FTIR (Multigas 2030, MKS instruments) at 453 K. The uncertainty in the gas analyzer measurements was below 10%. The error bars take into account analyzer uncertainty and formation of HCl on the reactor wall, but not any downstream loss of HCl or SO2. It was attempted to determine the degree of sulfation from the elemental composition of the collected fine particles, but the samples appeared to have been contaminated. For this reason, the degree of sulfation was quantified based on the SO2 and HCl measurements, as described below.

3. Chemical kinetic model

The detailed chemical kinetic model, i.e., the reaction mechanism and the thermodynamic data, is available as Supplementary Information. The core of the mechanism is based on the work of Glarborg and Marshall [24], with subsequent modifications by Hindiyarti et al. [26], Weng et al. [28], Vilchez et al. [30], and Chanpirak and coworkers [35, 43,45]. In addition to the potassium reactions, the model includes subsets for chlorine [46] and sulfur [26,44,47], as well as a reaction for homogeneous nucleation of K_2SO_4 [27]. Similar kinetic models are available for sulfation of sodium salts [24,48].

Table 1 lists the thermodynamic properties for selected species involved. Reliable thermodynamic data for the simpler potassium species (K, KO) and the salts (KCl, (KCl)2, KOH, K2SO4) are available from evaluations by Chase [49] and Gurvich et al. [50]. Also data for KO₂ [51] and KSO₂ [24,52] are fairly well established. However, in our present understanding, the sulfation reaction must involve a number of potassium species that have never been detected in the gas phase and for which few data are available. The thermodynamic data for these species (KClSO₃, KO_x, KSO_x, and KHSO_x; x = 3-4) were calculated theoretically by Marshall and coworkers [24,26,43]. The error margin in the predicted heats of formation for these species is $\pm 3-4$ kcal mol⁻¹ [24]. This level of accuracy is sufficient to ensure that species such as KClSO₃ and KHSO₄ have the required stability in the gas phase to act as precursors for K2SO4. However, the uncertainty affects the modeling predictions, since a number of reactions may proceed in the reverse direction or be close to partial equilibration.

Table 2 lists rate constants for key potassium reactions in the chemical kinetic model. The core of the alkali subset of the mechanism consists of reactions for which measurements are available, either for sodium or potassium [24]. The reported rate constants are typically large, often close to collision frequency in the exothermic direction of the reaction. This is true even for alkali reactions not involving radicals, such as NaOH + HCl \rightleftarrows NaCl + H₂O [55], since these steps exhibit ionic behavior. Based on this observation, the sulfation mechanism for KCl proposed by Glarborg and Marshall [24] had oxidation of SO₂ to SO₃ as the rate limiting step (SO₂ + O (+M) \rightarrow SO₃ (+M), SO₂ + OH (+M) \rightarrow HOSO₂ (+M), HOSO₂ + O₂ \rightarrow SO₃ + HO₂). The subsequent sulfation steps for KCl, i.e.,

$$KCl + SO_3(+M) \rightarrow KClSO_3(+M),$$
 (R13)

$$KCISO_3 + H_2O \rightleftarrows KHSO_4 + HCI$$
 (R20)

$$KHSO_4 + KCl \neq K_2SO_4 + HCl$$
 (R19)

are presumably all fast. The recombination of KCl with SO_3 , was calculated from ab initio theory by Glarborg and Marshall [24] to have a high rate constant, and k_{20} and k_{19} were assumed to be similar to the rate constant for NaOH + HCl. Notably, this sequence of alkali reactions does not involve radicals. However, radicals are required to promote the oxidation of SO_2 to SO_3 , which is otherwise very slow. Hindiyarti et al. [26] showed that the mechanism of Glarborg and Marshall was unable to predict sulfation reported at intermediate temperatures in the absence of combustibles [14].

To enhance the predicted sulfation under these conditions, Hindiyarti et al. [26] suggested two reaction sequences that allowed the sulfation to take place without SO_3 as an intermediate. The first sequence (A) involved KHSO $_3$ as an intermediate:

$$KOH + SO2(+M) \rightarrow KHSO3(+M)$$
 (R11)

$$KHSO_3 + O_2 \rightarrow KHSO_4 + O, \tag{R17b}$$

followed by completion of the sulfation through R19. This sequence involves only stable species as reactants and would be expected to have only a small sensitivity to the presence of combustibles such as CO. The

Table 1
Thermodynamic properties for selected potassium species. Units are kcal mol⁻¹ ($H_{f,298}$) and cal mol⁻¹ K^{-1} (S_{298} , C_p).

Species	$H_{f,298}$	S ₂₉₈	$C_{p,300}$	$C_{p,400}$	$C_{p,500}$	$C_{p,600}$	$C_{p,800}$	$C_{p,1000}$	$C_{p,1500}$	Ref.
K	21.27	38.32	4.97	4.97	4.97	4.97	4.97	4.97	5.00	[49,53]
KO	14.30	56.84	8.60	8.78	8.89	8.96	9.05	9.12	9.26	[26]
KO ₂	-22.74	64.15	11.56	12.13	12.56	12.88	13.27	13.47	13.69	[51]
кон	-53.00	56.90	11.77	12.21	12.47	12.62	12.83	13.07	13.62	[24,54]
KC1	-51.50	57.11	8.72	8.85	8.92	8.98	9.04	9.09	9.20	[24,54]
KSO ₂	-95.38	73.46	15.61	16.73	17.55	18.15	18.84	19.16	19.53	[24]
KSO ₃	-135.69	78.93	18.54	20.43	21.83	22.83	24.03	24.58	25.23	[24]
KSO ₄	-172.10	82.19	22.30	24.93	26.77	28.02	29.45	30.20	31.08	[43]
KHSO ₃	-164.69	81.01	21.56	23.85	25.45	26.55	27.87	28.69	29.93	[43]
KHSO ₄	-225.66	83.80	23.73	26.68	28.92	30.57	32.66	33.80	35.42	[24]
K ₂ SO ₄	-261.29	90.14	26.42	29.49	31.63	33.11	34.86	35.81	36.83	[24]
KClSO ₃	-189.73	86.25	23.30	25.37	26.92	28.07	29.47	30.17	31.01	[43]

Table 2
Rate coefficients for key reactions in the potassium subset. Units are cm, mol, s, K.

No	Reaction	A	n	E	Note	
1.	$K + O_2 + M \rightleftharpoons KO_2 + M$	3.3E21	-1.55	19	[51]	
2.	$K + HCl \rightleftharpoons KCl + H$	9.1E12	0.00	1 180	[56], ^a	
		1.0E14	0.00	3 635		
3.	$K + SO_2(+M) \rightleftarrows KSO_2(+M)$	3.7E14	0.00	0	[24,52]	
	Low pressure limit	5.2E23	-1.50	0		
4.	$K + SO_3(+M) \rightleftarrows KSO_3(+M)$	3.7E14	0.00	0	[24]	
	Low pressure limit	4.7E34	-4.90	0		
5.	$KO + H_2O \rightleftharpoons KOH + OH$	1.4E14	0.00	0	$NaO + H_2O [57,58]$	
6.	$KO + SO_2(+M) \rightleftarrows KSO_3(+M)$	3.7E14	0.00	0	$K + SO_2$ [24]	
	Low pressure limit	5.2E23	-1.50	0		
7.	$KO_2 + OH \rightleftharpoons KOH + O_2$	2.5E15	-0.16	0	[45]	
8.	$KO_2 + SO_2(+M) \rightleftarrows KSO_4(+M)$		Slow		pw	
9.	$KOH + H \rightleftharpoons K + H_2O$	2.3E13	0.00	0	NaOH + H [59]	
10.	$KOH + HCl \rightleftharpoons KCl + H_2O$	1.7E14	0.00	0	NaOH + HCl [24]	
11.	$KOH + SO_2(+M) \rightleftarrows KHSO_3(+M)$	1.0E14	0.00	0	$KOH + SO_3 [24,26]$	
	Low pressure limit	2.6E42	-7.60	0		
12.	$KOH + SO_3(+M) \rightleftarrows KHSO_4(+M)$	1.0E14	0.00	0	[24]	
	Low pressure limit	2.6E42	-7.60	0		
13.	$KCl + SO_3(+M) \rightleftarrows KClSO_3(+M)$	1.0E14	0.00	0	[24]	
	Low pressure limit	1.9E41	-7.80	0		
14.	$KSO_2 + O_2(+M) \rightleftharpoons KSO_4(+M)$		Slow		pw	
15.	$KSO_3 + OH + M \rightleftharpoons KHSO_4 + M$	1.0E23	-1.50	0	[26] est	
16.	$KHSO_4 + H \rightleftharpoons KHSO_3 + OH$	8.4E09	1.22	22 300	[28] est	
17.	$KHSO_4 + O \rightleftharpoons KHSO_3 + O_2$	2.0E12	0.00	0	pw	
18.	$KHSO_4 + KOH \rightleftharpoons K_2SO_4 + H_2O$	1.0E14	0.00	0	[24] est	
19.	$KHSO_4 + KCl \rightleftharpoons K_2SO_4 + HCl$	3.0E13	0.00	0	[30] est	
20.	$KCISO_3 + H_2O \rightleftharpoons KHSO_4 + HCI$	1.0E14	0.00	0	[24] est	
21.	$KCISO_3 + KOH \rightleftharpoons K_2SO_4 + HCI$	1.0E14	0.00	0	[24] est	
22.	$K_2SO_4 \rightarrow K_2SO_4(c)$	1.0E-61	0.00	-300 000	[27]	

^a Duplicate reaction: the rate constant is the sum of the two expressions.

rate limiting step is the KHSO $_3$ + O $_2$ reaction (R17b). The implication of this pathway is that it is the conversion of sulfite to sulfate, rather than oxidation of SO $_2$ to SO $_3$, which serves to oxidize SO $_2$ S^{IV} to a higher oxidation state.

The second sequence (B) suggested by Hindiyarti et al. involved KSO_4 as an intermediate:

$$K + O_2(+M) \rightarrow KO_2(+M) \tag{R1}$$

$$K + SO_2(+M) \rightarrow KSO_2(+M)$$
 (R3)

$$KO_2 + SO_2(+M) \rightarrow KSO_4(+M)$$
 (R8)

$$KSO_2 + O_2(+M) \rightarrow KSO_4(+M) \tag{R14}$$

$$KSO_4 + H_2O \rightarrow KHSO_4 + OH$$
,

followed by R19. As it involves several radicals, this sequence would be promoted in the presence of CO, because its combustion would facilitate development of a radical pool.

The rate constants for the additional sulfation steps proposed by Hindiyarti et al. were largely just guesses, and several values have been revised in subsequent work [28,30]. In the present work, we have re-evaluated these two pathways to sulfation. In sequence A, the rate limiting step is KHSO₃ + O₂ (R17b). In the mechanism, it is represented in the reverse, exothermic direction as KHSO₄ + O \rightleftharpoons KHSO₃ + O₂ (R17). Hindiyarti et al. assumed that $k_{17} \sim 1 \cdot 10^{13}$ cm³ mol $^{-1}$ s $^{-1}$, roughly equal to the rate constant for NaO₂ + O \rightarrow NaO + O₂ [60]. More recently, Weng et al. [28] estimated k_{17} from analogy with the SO₃ + O reaction, resulting in a value several orders of magnitude lower, in effect eliminating sequence A.

In the present work, the rate constant for R17 is estimated from modeling of KCl sulfation experiments in the absence of combustibles. Under these conditions, sequence A is responsible for the sulfation and reaction 17b is the rate controlling step. As discussed further below, a range of sulfation results obtained by different groups under different conditions can be interpreted satisfactorily by the model in terms of $k_{17} \approx 2 \cdot 10^{12} \ cm^3 \ mol^{-1} \ s^{-1},$ independent of temperature, and this value is adopted in the mechanism.

To evaluate the importance of the KSO_4 reaction pathway (sequence B), reactions $KO_2 + SO_2$ (+M) \rightarrow KSO_4 (+M) (R8) and $KSO_2 + O_2$ (+M) \rightarrow KSO_4 (+M) (R14) were investigated with density functional theory, at the B3LYP/6-31G(2df,p) level of theory [61]. Attempts to find transition states for these exothermic processes yielding KSO_4 were

unsuccessful. Relaxed scans for various approaches of the reactant pairs indicated repulsive interactions, and that collision energies above ${\sim}20~\rm kcal~mol^{-1}$ would be needed. Accordingly we expect sequence B to be negligibly slow. We did discover an alternative pathway, where $\rm KO_2 + \rm SO_2$ is connected to $\rm KSO_2 + \rm O_2$ via a weakly bound $\rm SO_2 \rm KO_2$ intermediate. The K atom lies across the two pairs of O atoms with K-O distances of $\rm 2.7 \times 10^{-10}$ m. This species could provide a path for coupling $\rm KO_2$ and $\rm KSO_2$ exchange, but G4 calculations [61] indicate that $\rm SO_2 \rm KO_2$ is endothermic relative to $\rm KO_2 + \rm SO_2$ by ca. 5 kcal mol $^{-1}$ at 298 K. Interconversion via this metastable isomer of $\rm KSO_4$ will not be fast.

4. Results and discussion

4.1. Present experiments

In the present work, the sulfation of KCl by SO_2 was investigated in the presence and absence of CO in a laminar flow reactor. The experiments were conducted with a lean $KCl/O_2/H_2O/SO_2$ mixture w/wo CO, strongly diluted in N_2 . The KCl inlet level was about 200 ppm, with 750 ppm SO_2 , and 0 and 500 ppm CO and 5% O_2 . The KCl feeding concentration was determined from knowledge of the solution strength together with the measured water vapor level in the outlet. The very fuel-lean conditions are representative for burnout conditions in a post-flame zone. In addition, results for 1000 ppm CO under otherwise similar conditions were adopted from Chanpirak et al. [43].

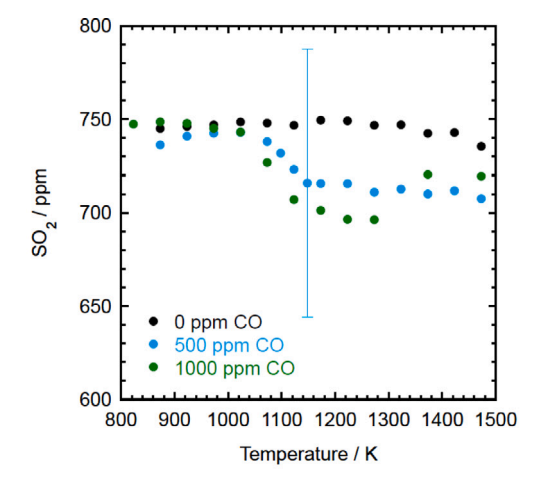
Fig. 2 shows experimental results for SO_2 and HCl, respectively, for the investigated conditions. In the absence of CO, the SO_2 consumption is very small (upper figure). For 500 and 1000 ppm CO, up to a maximum of 50 ppm SO_2 is consumed in the 1050-1350 K range. For an isolated data point, the SO_2 consumption is within the measurement uncertainty (10% of the concentration), but the relative difference between data points is more reliable. Based on repetitions of experiments (see Supplementary Material), we estimate the error in ΔSO_2 to be less than 50%.

The HCl formation (lower figure) is of the order of 0-20 ppm in the absence of CO, while it reaches peak values of around 60 ppm in the presence of 500-1000 ppm CO. Hydrogen chloride is primarily formed by the sulfation reaction. According to modeling predictions, the KCl + $H_2O \rightleftharpoons KOH + HCl$ reaction (R10b) is rapidly equilibrated under the present conditions, but yields only a minor amount of HCl. However, HCl can also be formed from the heterogeneous reaction of KCl with SiO₂ at the quartz reactor surface. Both Krum et al. [34] and Chanpirak et al. [43] have reported formation of HCl when reacting a KCl/H₂O/O₂ mixture at high temperature in a quartz tube. The HCl formation was independent of [O₂] but varied with temperature, peaking at temperatures in the 1100-1200 K range. Under conditions similar to the present work, Chanpirak et al. detected peak levels of 10-15 ppm HCl in the absence of SO₂. The error bars shown in the figures below account for both analyzer uncertainty and conversion of KCl to HCl on the reactor quartz wall.

The overall reaction for sulfation of KCl can be written as 2KCl + $SO_2 + \frac{1}{2}O_2 + H_2O \longrightarrow K_2SO_4 + 2HCl$. The sulfation thus consumes SO_2 while it yields gaseous HCl, along with potassium sulfate aerosols that can be captured downstream in the filter. These results show that the CO oxidation, which replenishes the radical pool, serves to promote the conversion of KCl.

Both the SO_2 and HCl concentrations in the product gas and the content of S in the filter sample are measures of the degree of sulfation. In the present work, the sulfation degree could not be determined reliably from the elemental composition of the collected fine particles due to problems with contamination. For this reason, the sulfation was quantified based on the SO_2 and HCl measurements.

Fig. 3 compares experimental results for the degree of KCl sulfation as a function of temperature and CO inlet level. There is a significant scatter in the sulfation data, but the results based on the HCl and



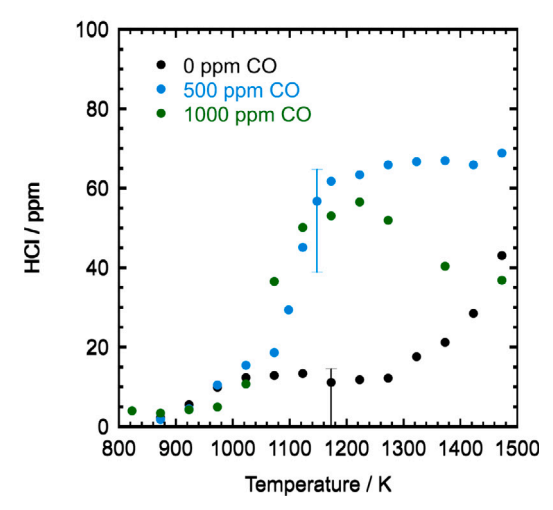


Fig. 2. Measured mole fractions of SO_2 (upper figure) and HCl (lower figure) as a function of temperature and CO inlet concentration in the CO/KCl/ $SO_2/O_2/H_2O$ system. Inlet conditions: 0, 500, or 1000 ppm CO, 212 ppm KCl, 750 ppm SO_2 , 5% O_2 , 3.2% H_2O ; N_2 balance. The data for 1000 ppm CO were drawn from Chanpirak et al. [43]. The pressure was atmospheric and the residence time was 92/T(K) in the isothermal zone.

 SO_2 measurements agree within the combined uncertainty. For the conditions with 1000 ppm CO [43] (Fig. 3 lower), the sulfation degree was estimated as well from chemical analysis of the aerosols captured downstream in the filter. This method yields slightly lower values than the gas measurements, but the level of agreement lends credibility to the quantification.

In the absence of CO, sulfation of KCl is small below 1300 K, increasing with temperature above this value. The presence of 500 or 1000 ppm CO clearly promotes the sulfation, which increases strongly already at 1100 K. The 500 ppm CO data suggest a plateau in the degree of sulfation above 1100 K, while results obtained with 1000 ppm CO show a peak, followed by lower conversion at the highest temperatures. The difference is attributed to the experimental uncertainty, rather than a strong impact of the CO level.

Calculations are shown only for temperatures above 1000 K; below this value the KCl feed may not be fully vaporized and there is a competition between gas-phase and condensed-phase sulfation. Taking into account the significant experimental uncertainty, the modeling predictions are in satisfactory agreement with observations. The strongly improved accuracy in the presence of CO, compared to the recent modeling of Chanpirak et al. [43], is due to the elimination of the KSO4 pathway and the updated rate constant for reaction R17 in the present work.

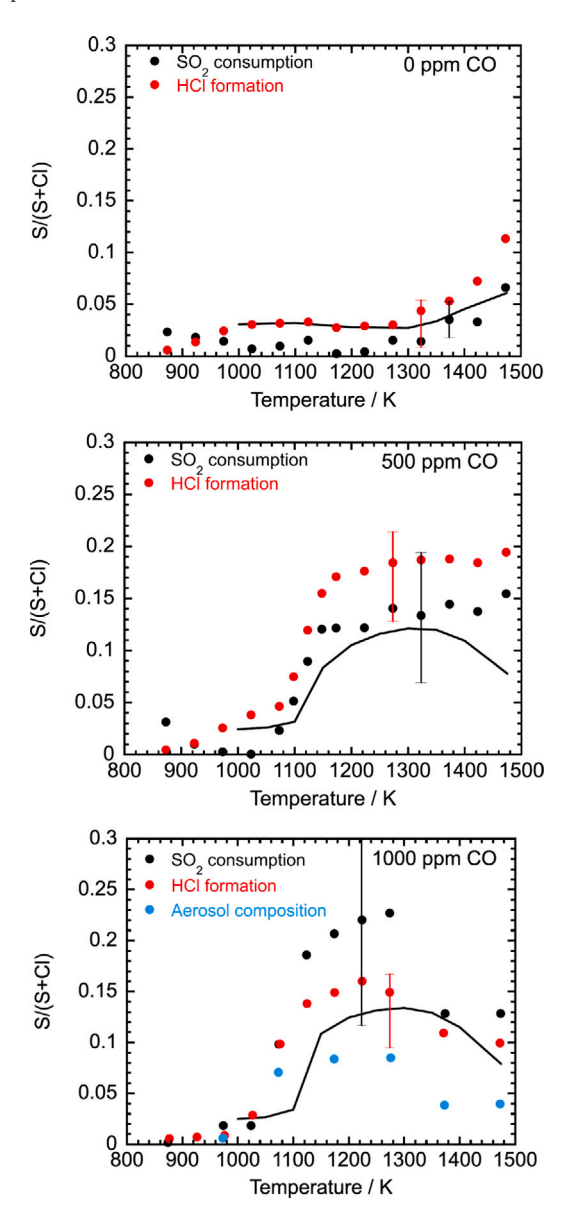


Fig. 3. Comparison of experimental and predicted molar ratios of S/(Cl+S) in the aerosols based on the SO_2 consumption, the HCl formation, and (for 1000 ppm CO) analysis of collected particle samples. Inlet conditions: 0, 500, or 1000 ppm CO, 212 ppm KCl, 750 ppm SO_2 , 5% O_2 , 3.2% H_2O ; N_2 balance. Symbols denote experimental data; lines denote modeling predictions with the present model. The pressure was atmospheric and the residence time was 92/T(K) in the isothermal zone.

Fig. 4 shows modeling predictions for CO and HCl for a temperature of 1273 K and 1000 ppm CO in the inlet. The reaction KCl + $\rm H_2O \rightleftharpoons$ KOH + HCl reaction (R10b), which is rapidly equilibrated, is reponsible for the almost instantaneous formation of about 5 ppm of HCl. The subsequent HCl formation originates from the sulfation reaction. According to the calculations, the sulfation rate peaks during CO oxidation; once CO is depleted, the conversion of potassium is limited by the rate of oxidation of sulfite to sulfate, which is comparatively slow. The modeling supports a peak in sulfation at around 1300 K; above this temperature thermodynamic constraints limit the gas-phase sulfation.

4.2. Experiments from literature

In addition to modeling the current experiments, the updated detailed gas phase mechanism is used to simulate the conditions of

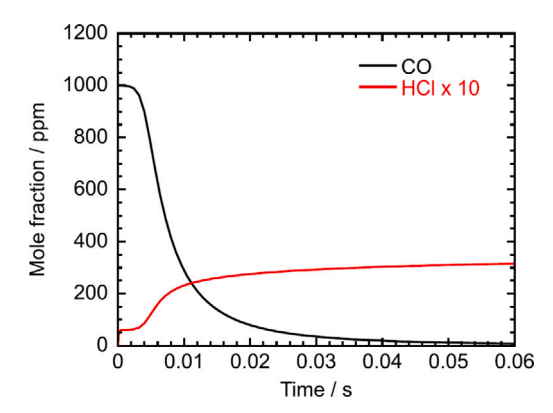


Fig. 4. Predicted concentration profiles of CO and HCl as a function of time at 1273 K for an inlet composition with 1000 ppm CO, 212 ppm KCl, 750 ppm SO_2 , 5% O_2 , 3.2% H_2O (corresponding to Fig. 2 lower).

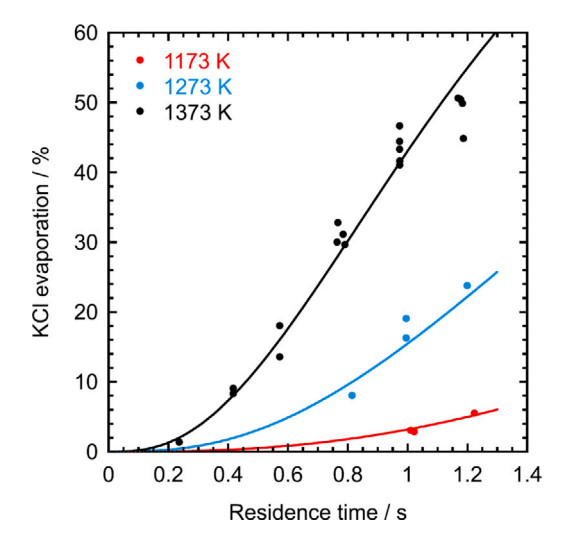


Fig. 5. Degree of vaporization of the solid KCl particles in the entrained flow reactor at 1373 K. Symbols denote experimental results [23]; solid line denotes predictions with a simplified vaporization model. KCl(s) feed, 0.24 g/min; total gas flow 10–20 Nl/min.

experimental work from Iisa et al. [23], Jensen et al. [14] and Jimenez and Ballester [18].

The experiments from lisa et al. were conducted at temperatures of 1173, 1273, and 1373 K in an entrained flow reactor. Solid KCl particles were introduced to the system together with a gas mixture consisting of SO_2 , O_2 , H_2O , and N_2 to balance. The gas residence time in the isothermal part of the reactor was in range from 0.3–1.5 s, after which a quenching system was applied to avoid further reaction.

The modeling was conducted in two steps. First, the evaporation of solid potassium chloride was modeled as three pseudo-first order reactions in series, following the approach of Glarborg and Marshall [24]. The rate constants were fitted to match the experimental data by Iisa et al. A comparison between the observed and predicted degrees of KCl vaporization as a function of residence time is shown in Fig. 5 for temperatures of 1173–1373 K.

The sulfation degree was then modeled using the full mechanism, including the pseudo-reactions describing KCl evaporation. Fig. 6 compares the S/(S+Cl) ratio in the captured fine particles measured by Iisa et al. as a function of the residence time and temperature in the entrained flow reactor with modeling predictions. The cooling rate was not reported by Iisa et al. and an estimated value was employed in the calculations. The aerosol formation takes place during cooling, but the calculated sulfation degree has only a limited sensitivity to the assumed

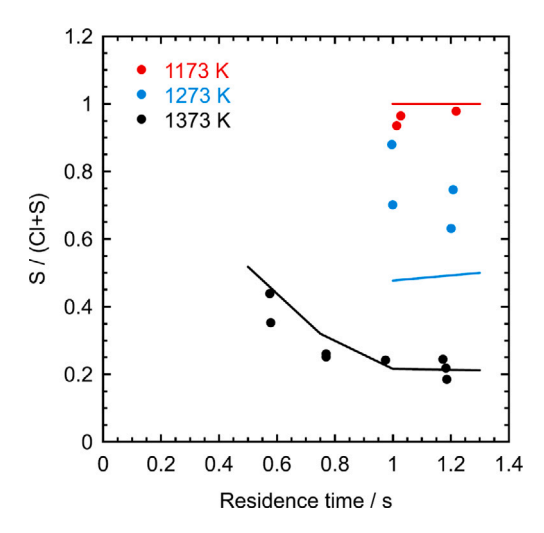


Fig. 6. Comparison of model predictions (solid lines) with the experimental data (symbols) from lisa et al. [23] for the S/(S+Cl) ratio in the fine particles as a function of residence time in an entrained flow reactor. Experimental conditions: temperature 1173-1373 K; KCl(s) feed 0.24 g/min; total gas flow 10 Nl/min; 2% SO₂, 5% O₂, 10% H₂O, balance N₂.

cooling rate, decreasing slightly with higher values. The conversion of KCl is seen to decrease as a function of time, most pronounced at 1273 K and 1373 K. This is a result of the competition between vaporization of KCl and sulfation. The sulfation rate is comparatively fast initially but becomes slower with time, while the KCl evaporation rate is more or less constant. The model captures almost quantitatively the degree of sulfation at 1173 K (close to full conversion) and at 1373 K, while at 1273 K the conversion of KCl is underpredicted.

Fig. 7 shows the effect of the inlet concentrations of SO_2 , O_2 , and H_2O , respectively, on the sulfation of KCl at 1373 K. The results show that even though sulfur dioxide in all experiments is present in considerable excess compared to the potassium concentration, the formation of K_2SO_4 increases significantly with the SO_2 level (Fig. 7 upper). Iisa et al. [23] took this to indicate that formation of SO_3 is a rate-limiting step in the sulfation process. However, in our present understanding, it is the oxidation of sulfite to sulfate that controls the sulfation rate (in the absence of combustion). The modeling predictions are in good agreement with the experimental results, except at the highest SO_2 level, where the potassium sulfate formation is underpredicted.

Fig. 7 (middle) shows the effect of the inlet $\rm O_2$ concentration on $\rm K_2SO_4$ formation. Even though the degree of sulfation is slightly underpredicted at the lowest oxygen level, the model captures the experimental trend well. The degree of sulfation increases with the oxygen level, but not as strongly as with the sulfur dioxide level. Fig. 7 (lower) shows the effect of the water vapor concentration. Here the experimental observations indicate that the sulfation rate is largely independent of $\rm [H_2O]$, while the model predicts a slight increase in $\rm [K_2SO_4]$ with increasing water vapor level. However, the discrepancy between the experimental data and the modeling predictions is within the experimental uncertainty.

Modeling predictions are also compared to the experimental data from Jensen et al. [14] . They conducted experiments in a laboratory tubular flow reactor using a synthetic flue gas containing a mixture of gaseous KCl, SO_2 , O_2 , and H_2O vapor, highly diluted in N_2 . Potassium chloride was added to the system by saturating part of the feed stream with a salt vapor. The peak temperature was varied between 1043 and 1273 K. The temperature profile is shown in Fig. 8.

The experimental data, presented as the S/(S+Cl) ratio in the aerosol, are shown in Fig. 9. The impact of the peak temperature on the sulfation rate is small. The model captures well the degree of sulfation over the range of temperature investigated.

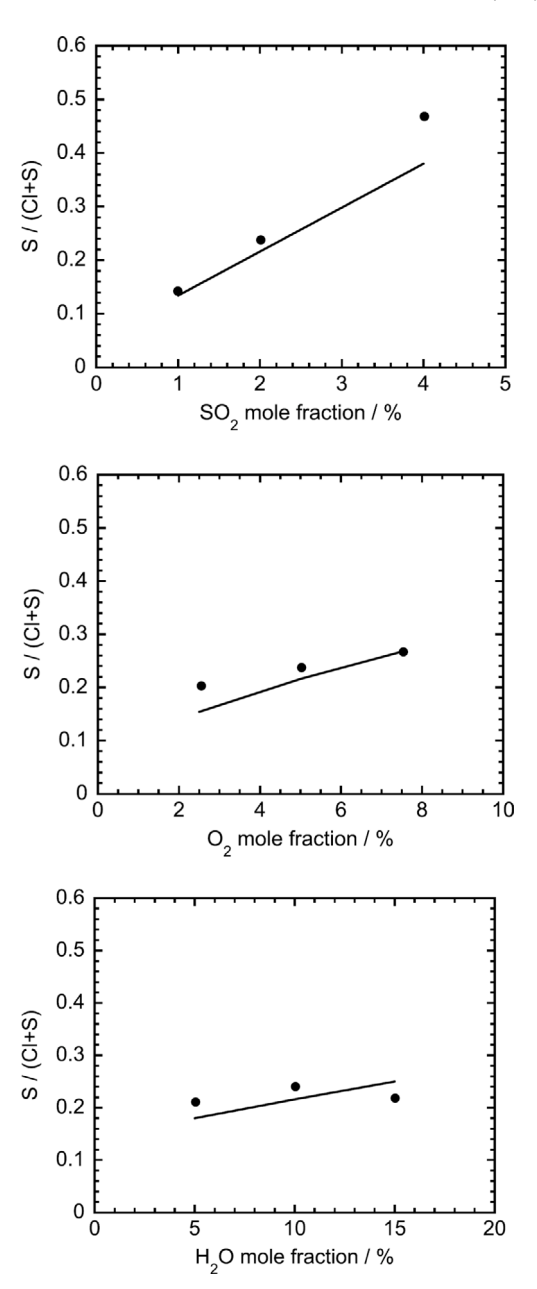


Fig. 7. Comparison of model predictions (solid lines) with the experimental data (symbols) from Iisa et al. [23] for the S/(S+Cl) ratio in the fine particles as a function of the SO₂ concentration in an entrained flow reactor. Baseline experimental conditions: temperature 1373 K; KCl(s) feed 0.24 g/min; total gas flow 10 Nl/min; 2% SO₂, 5% O₂, 10% H₂O, balance N₂. *Upper figure*: 1%–5% SO₂; *Middle figure*: 2.5–7.5% O₂; *Lower figure*: 5%–15% H₃O. The residence time in the isothermal zone is approximately 1 s.

Finally, the model is evaluated against experimental data from Jimenez and Ballester [18,25] for combustion of orujillo in an entrained flow reactor. The reactor involved an isothermal section with a temperature of 1573 K, followed by a cooling section with a temperature gradient of $\sim\!600$ K/s. The isothermal zone residence time was about 0.3 s. A comparison between modeling predictions and the observed Cl/S ratio in the aerosols is presented in Fig. 10. The model predicts correctly full sulfation of the potassium for levels of about 200 ppm SO₂ and higher. However, it strongly underpredicts the degree of sulfation at very low SO₂ levels (10–25 ppm).

There are some experimental effects that may have promoted the sulfation rate at low concentrations of SO_2 . Coal fly ash has been reported to catalyze the oxidation of SO_2 to SO_3 [62–64]. To our

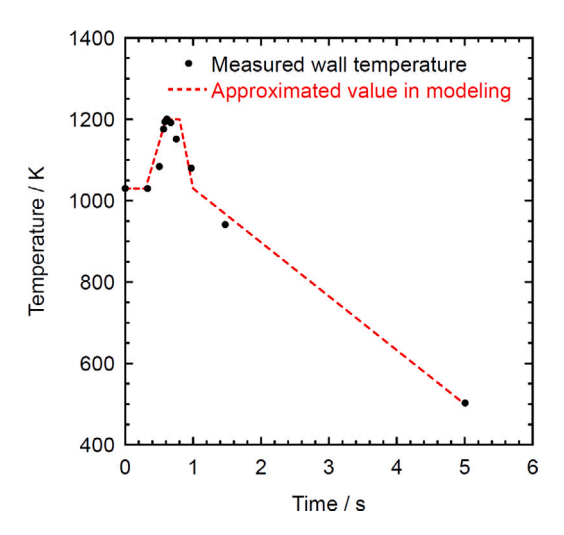


Fig. 8. The measured wall temperature as a function of residence time in the flow reactor experiments from Jensen et al. [14] and comparison with the approximated temperature profile used in the calculations.

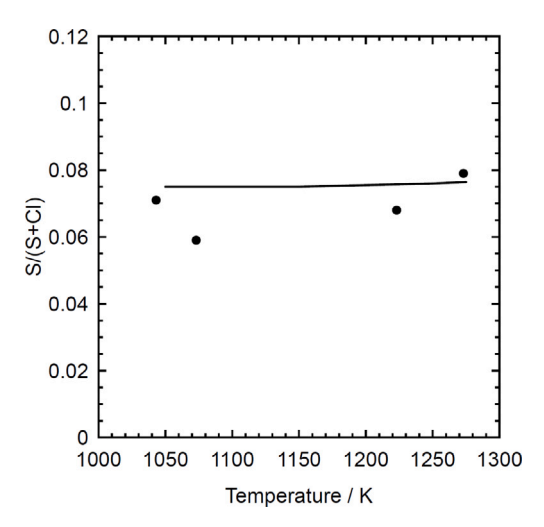


Fig. 9. Comparison of model predictions (solid line) with the experimental data from Jensen et al. [14] for the S/(S+Cl) ratio in the fine particles as a function of peak temperature in a flow reactor. The reactant gas is heated to the peak temperature, followed by cooling. Inlet composition: 200 ppm KCl, 200 ppm SO_2 , 4% O_2 , 4.2% H_2O_3 ; balance N_2 .

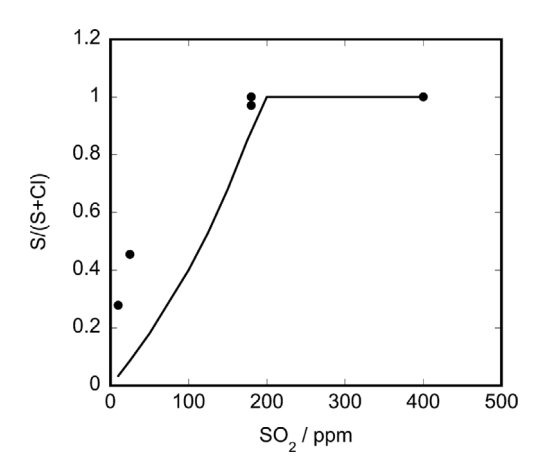


Fig. 10. Comparison of model predictions (solid line) with experimental data for the sulfation degree of the captured aerosol particles in combustion of orujillo in an entrained flow reactor. The experimental results are from Jimenez and Ballester [18,25]. Inlet composition: 13 ppm KOH, 34 ppm HCl, 10–400 ppm SO_2 , 5% O_2 , 20% H_2O , 8% CO_2 ; balance N_2 .

knowledge, there are no investigations of the reactivity of biomass fly ash. However, it is conceivable that the fly ash particles could promote SO₂ oxidation in the cooling zone of the entrained flow reactor, facilitating sulfation. Presence of unburned char during cooling, leading to formation of CO, could have a similar effect. The particle range used in the entrained flow reactor experiments was 300-400 µm [18,25]. The 400 µm particles would have a char oxidation time at 1573 K of approximately one second, assuming diffusion-limited oxidation, so it is likely that some unburned char would remain at the end of the isothermal region. Char oxidation in the cooling region would give rise to formation and combustion of CO, which promotes oxidation of SO_2 to SO_3 and thereby sulfation. At the lowest level of SO_2 in the experiments (10 ppm), it would take a conversion of SO₂ to SO₃ during cooling of only about 25%, facilitated by either fly ash catalysis or CO oxidation, to explain the observed degree of sulfation. However, these effects are difficult to quantify. Controlled laboratory experiments on sulfation of KCl at low levels of SO2 would be desirable, but they could not be conducted as part of the present work due to the diagnostic limitations.

4.3. Kinetic analysis

Fig. 11 shows a reaction path diagram for sulfation of KCl w/wo presence of CO. In the absence of CO (solid lines), radical levels are low. This inhibits the oxidation of SO_2 to SO_3 and in our current understanding, it is the oxidation of sulfite (KHSO₃) to sulfate (KHSO₄), which serves to oxidize SO_2 S^{IV} to a higher oxidation state. The sulfation takes place mainly through the following sequence of reactions:

$$KCl + H_2O \rightarrow KOH + HCl$$
 (R10b)

$$KOH + SO2(+M) \rightarrow KHSO3(+M)$$
 (R11)

$$KHSO_3 + O_2 \rightarrow KHSO_4 + O \tag{R17b}$$

$$KHSO_4 + KCl \rightarrow K_2SO_4 + HCl$$
 (R19)

This sequence, originally proposed by Hindiyarti et al. [26], does not involve any radicals. The rate limiting step is the oxidation of $KHSO_3$ to $KHSO_4$.

When a combustible such as CO is added to the reactants, the oxidation acts to replenish the radical pool and opens up other sulfation pathways for KCl. The most significant effect is that SO₂ is now partly oxidized to SO₃, mostly through the reaction,

$$SO_2 + O(+M) \rightarrow SO_3(+M)$$

The SO₃ promotes the conversion of KCl to KHSO₄, either via KClSO₃

$$KCl + SO_3(+M) \rightarrow KClSO_3(+M),$$
 (R13)

$$KCISO_3 + H_2O \rightarrow KHSO_4 + HCI$$
 (R20)

or through KOH,

$$KOH + SO_3(+M) \rightarrow KHSO_4 + HCl$$
 (R12)

This reaction sequence, followed by conversion of KHSO $_4$ to K $_2$ SO $_4$ through R19, is the sulfation pathway originally proposed by Glarborg and Marshall [24]. However, according to the model, the increased radical concentrations also facilitate smaller pathways to sulfation involving K and KO, both through KSO $_3$: KCl + H \rightarrow K + HCl (R2b), K + SO $_3$ (+M) \rightarrow KSO $_3$ (+M) (R4) or KOH + OH \rightarrow KO + H $_2$ O (R5b), KO + SO $_2$ (+M) \rightarrow KSO $_3$ (+M) (R6), followed by recombination of KSO $_3$ with OH to form KHSO $_4$ (R15).

Notably, in the presence of CO (i.e., at higher radical levels), KHSO $_4$ is consumed, rather than formed, from reaction R17: KHSO $_4$ + O \rightarrow KHSO $_3$ + O $_2$ (R17). The KHSO $_3$ then decomposes thermally to KOH + SO $_2$ (R12b).

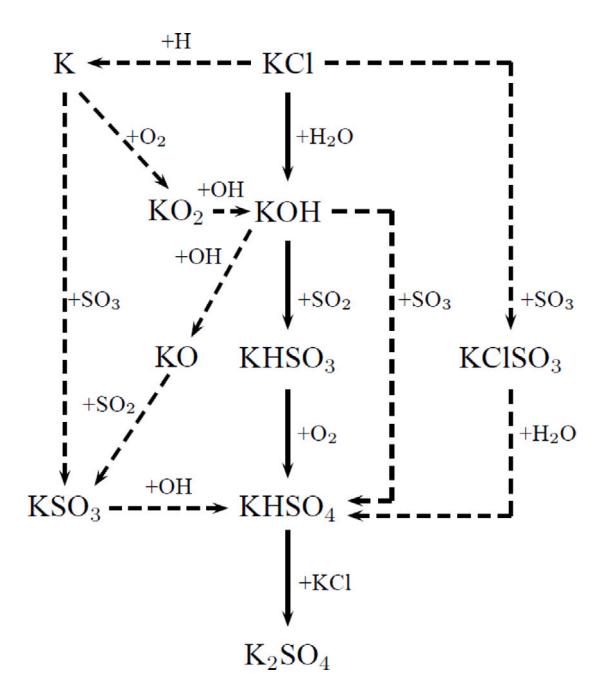


Fig. 11. Reaction path diagram for sulfation of KCl in the absence (solid lines) and presence (dashed lines) of CO.

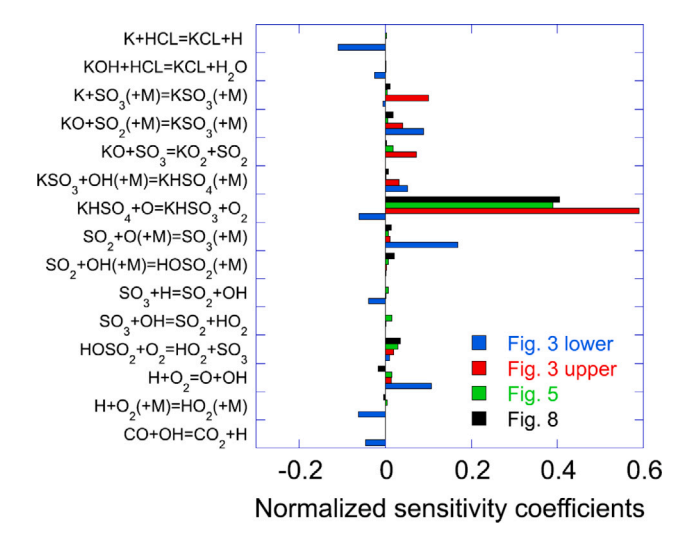


Fig. 12. Sensitivity of the predicted K_2SO_4 formation to key reactions in the mechanism. Conditions correspond to flow reactor experiments from the present work (Fig. 3 upper (0 ppm CO) and lower (1000 ppm CO)), from Iisa et al. [23] (Fig. 6), and from Jensen et al. [14] (Fig. 9); all for a peak temperature of 1273 K. (For interpretation of the references to color in this figure legend, the reader is referred to the web version of this article.)

Fig. 12 shows a sensitivity analysis for the predicted K_2SO_4 formation. The calculations were conducted at a temperature of 1273 K for the conditions of Fig. 3 (present reactor experiments), Fig. 6 (Iisa et al. [23]), and Fig. 9 (Jensen et al. [14]). The blue bars represent the 1000 ppm CO conditions of Fig. 3, while all the other coefficients are for experiments without CO.

In the absence of CO, the sulfite to sulfate reaction, KHSO $_3$ + O $_2$ \rightarrow KHSO $_4$ + O (R17b), exhibits by far the highest sensitivity coefficients, confirming that this is the main rate limiting step when no combustion is taking place. Reactions in the sequence K + SO $_3$ (+M) \rightarrow KSO $_3$ (+M) (R4), KO + SO $_2$ (+M) \rightarrow KSO $_3$ (+M) (R6), KSO $_3$ + OH (+M) \rightarrow KHSO $_4$ (+M) (R15), a minor sulfation pathway, also show up with positive sensitivity coefficients.

In the presence of CO (blue bars), more reactions show up as important. The most sensitive step is the recombination of SO_2 with O to form SO_3 . Reactions that form atomic oxygen, mainly $H+O_2\to O+OH$, promote sulfation, while steps that consume O (KHSO $_4+O$ (R17)) or compete with $H+O_2$ ($H+O_2+M$) exhibit negative coefficients. The SO_3+H reaction, along with steps forming atomic hydrogen (K+HCl, CO+OH), serve to inhibit sulfation.

5. Conclusions

Through a combined experimental, theoretical, and chemical kinetic modeling study, the gas-phase sulfation of KCl by SO2 has been reexamined. Particular emphasis was put on the effect of the radical pool on the sulfation pathways. Flow reactor experiments on KCl sulfation with and without addition of CO showed that oxidation of combustibles, facilitating establishment of a radical pool, strongly promotes sulfation. In this case, the sulfation rate is controlled by the oxidation of SO_2 to SO_3 , mostly through $SO_2 + O(+M) \rightarrow SO_3(+M)$. In the absence of combustibles, the rate limiting step in the sulfation appears to be the oxidation of potassium sulfite to potassium sulfate through KHSO₃ + O₂ \rightarrow KHSO₄ + O (R17b). With an estimated value of $k_{17} \sim 2 \cdot 10^{12} \text{ cm}^3 \text{ mol}^{-1} \text{ s}^{-1}$, the chemical kinetic model predicts the degree of sulfation satisfactorily over a range of experimental techniques and reaction conditions. An alternative sulfation pathway involving KSO₄ as an intermediate was discarded, because the formation through either KO₂ + SO₂ or KSO₂ + O₂ was found to involve significant barriers to reaction.

CRediT authorship contribution statement

Arphaphon Chanpirak: Writing – original draft, Investigation, Formal analysis, Data curation. **Hao Wu:** Conceptualization. **Paul Marshall:** Writing – review & editing, Conceptualization. **Peter Glarborg:** Writing – review & editing, Conceptualization.

Declaration of competing interest

The authors declare that they have no known competing financial interests or personal relationships that could have appeared to influence the work reported in this paper.

Data availability

Data will be made available on request.

Acknowledgments

This work was supported by Ørsted Bioenergy & Thermal Power A/S. PM thanks the National Science Foundation for computational facilities purchased under award OAC-2117247.

Appendix A. Supplementary data

Supplementary material related to this article can be found online at https://doi.org/10.1016/j.fuel.2024.130974.

References

- Olsson JG, Jäglid U, Pettersson JBC, Hald P. Alkali metal emission during pyrolysis of biomass. Energy Fuels 1997;11:779–84.
- [2] Knudsen JN, Jensen PA, Lin W, Frandsen FJ, Dam-Johansen K. Sulfur transformations during thermal conversion of herbaceous biomass. Energy Fuels 2004:18:810-9
- [3] Knudsen JN, Jensen PA, Dam-Johansen K. Transformation and release to the gas phase of Cl, K, and S during combustion of annual biomass. Energy Fuels 2004;18:1385–99.
- [4] Knudsen JN, Jensen PA, Lin W, Dam-Johansen K. Secondary capture of chlorine and sulfur during thermal conversion of biomass. Energy Fuels 2005;19:606–17.
- [5] van Lith SC, Alonso-Ramírez V, Jensen PA, Frandsen FJ, Glarborg P. Release to the gas phase of inorganic elements during wood combustion. Part 1: development and evaluation of quantification methods. Energy Fuels 2006;20:964–78.
- [6] van Lith SC, Alonso-Ramírez V, Jensen PA, Frandsen FJ, Glarborg P. Release to the gas phase of inorganic elements during wood combustion. Part 2: influence of fuel composition. Energy Fuels 2008;22:1598–609.
- [7] Johansen JM, Jakobsen JG, Frandsen FJ, Glarborg P. Release of K, Cl, and S during pyrolysis and combustion of high-chlorine biomass. Energy Fuels 2011;25:4961–71.
- [8] Jenkins BM, Baxter LL, Miles Jr TR, Miles TR. Combustion properties of biomass. Fuel Process Technol 1998;54:17–46.
- [9] Werther J, Saenger M, Hartge E-U, Ogada T, Siagi Z. Combustion of agricultural residues. Prog Energy Combust Sci 2000;26:1–27.
- [10] Niu Y, Tan H, Hui S. Ash-related issues during biomass combustion: Alkaliinduced slagging, silicate melt-induced slagging (ash fusion), agglomeration, corrosion, ash utilization, and related countermeasures. Prog Energy Combust Sci 2016;52:1–61.
- [11] Hupa M, Karlstrom O, Vainio E. Biomass combustion technology development -It is all about chemical details. Proc Combust Inst 2017;36:113–34.
- [12] Christensen KA, Stenholm M, Livbjerg H. The formation of submicron aerosol particles, HCl and SO, in straw-fired boilers. J Aerosol Sci 1998:29:421-44.
- [13] Christensen KA, Livbjerg H. A plug flow model for chemical reactions and aerosol nucleation and growth in an alkali-containing flue gas. Aerosol Sci Technol 2000;33:470–89.
- [14] Jensen JR, Nielsen LB, Schultz-M
 øller C, Wedel S, Livbjerg H. The nucleation of aerosols in flue gases with a high content of alkali - A laboratory study. Aerosol Sci Technol 2000;33:490–509.
- [15] Nielsen HP, Baxter LL, Sclippab G, Morey C, Frandsen FJ, Dam-Johansen K. Deposition of potassium salts on heat transfer surfaces in straw-fired boilers: A pilot-scale study. Fuel 2000;79:131–9.
- [16] Frandsen FJ. Utilizing biomass and waste for power production—a decade of contributing to the understanding, interpretation and analysis of deposits and corrosion products. Fuel 2005;84:1277–94.
- [17] Karlsson S, Pettersson J, Johansson L-G, Svensson J-E. Alkali induced high temperature corrosion of stainless steel: the influence of NaCl, KCl and CaCl₂. Oxid Met 2012;78:83–102.
- [18] Jiménez S, Ballester J. Influence of operating conditions and the role of sulfur in the formation of aerosols from biomass combustion. Combust Flame 2005;140:346–58.
- [19] Hu Z, Wang X, Ruan R, Li S, Bai S, Zhang J, Tan H. Effect of SO₂ addition on PM formation from biomass combustion in an entrained flow reactor. Energy Fuels 2018;32:11030–7.
- [20] Wang X, Hu Z, Adeosun A, Liu B, Ruan R, Li S, Tan H. Particulate matter emission and K/S/Cl transformation during biomass combustion in an entrained flow reactor. J Energy Inst 2018;91:835–44.
- [21] Pettersson J, Folkeson N, Johansson L-G, Svensson J-E. The effects of KCl $\rm K_2SO_4$ and $\rm K_2CO_3$ on the high temperature corrosion of a 304-type austenitic stainless steel. Oxid Met 2011;76:93–109.
- [22] Christensen KA, Livbjerg H. A field study of submicron particles from the combustion of straw. Aerosol Sci Technol 1996;25:185–99.
- [23] Iisa K, Lu Y, Salmenoja K. Sulfation of potassium chloride at combustion conditions. Energy Fuels 1999;13:1184–90.
- [24] Glarborg P, Marshall P. Mechanism and modeling of the formation of gaseous alkali sulfates. Combust Flame 2005;141:22–39.
- [25] Jiménez S, Ballester J. Formation of alkali sulphate aerosols in biomass combustion. Fuel 2007;86:486–93.
- [26] Hindiyarti L, Frandsen FJ, Livbjerg H, Glarborg P, Marshall P. An exploratory study of alkali sulfate aerosol formation during biomass combustion. Fuel 2008;87:1591–600.
- [27] Li B, Sun Z, Li Z, Aldén M, Jakobsen JG, Hansen S, Glarborg P. Post-flame gas-phase sulfation of potassium chloride. Combust Flame 2013;160:959–69.
- [28] Weng W, Chen S, Wu H, Glarborg P, Li Z. Optical investigation of gas-phase KCl/KOH sulfation in post flame conditions. Fuel 2018;224:461–8.
- [29] Weng W, Zhang Y, Wu H, Glarborg P, Li Z. Optical measurements of KOH, KCl and K for quantitative K-Cl chemistry in thermochemical conversion processes. Fuel 2020;271:117643.

- [30] Vilches TB, Weng W, Glarborg P, Li Z, Thunman H, Seemann M. Shedding light on the governing mechanisms for insufficient CO and H₂ burnout in the presence of potassium, chlorine and sulfur. Fuel 2020;273:117762.
- [31] Weng W, Li Z, Wu H, Aldén M, Glarborg P. Quantitative K-Cl-S chemistry in thermochemical conversion processes using in situ optical diagnostics. Proc Combust Inst 2021;38:5219–27.
- [32] Wu H, Jespersen JB, Frandsen FJ, Glarborg P, Aho M, Paakkinen K, Taipale R. Modeling of ferric sulfate decomposition and sulfation of potassium chloride during grate-firing of biomass. AIChE J 2013;59:4314–24.
- [33] Wu H, Pedersen MN, Jespersen JB, Aho M, Roppo J, Frandsen FJ, Glarborg P. Modeling the use of sulfate additives for potassium chloride destruction in biomass combustion. Energy Fuels 28:2013.
- [34] Krum KKR, Jensen MP, Li S, Norman T, Marshall P, Wu H, Glarborg P. Selective non-catalytic reduction of NO_x using ammonium sulfate. Energy Fuels 2021:35:12392-402
- [35] Chanpirak A, Jensen MKK, Wu H, Glarborg P. Sulfation of gaseous KCl by H₂SO₄. Energy Fuels 2023;37:2319–28.
- [36] Sengeløv LW, Hansen TB, Bartolome C, Wu H, Pedersen KH, Frandsen FJ, Jensen AD, Glarborg P. Sulfation of condensed potassium chloride by SO₂. Energy Fuels 2013;27:3283–9.
- [37] Capablo J, Ballester J. Experimental study of the kinetics of sulfation of alkali chloride deposits. Fuel Process Technol 2015;140:215–21.
- [38] Garba DB, Ma L, Porter RTJ, Pourkashnian M, Tan HZ, Williams A. Prediction of potassium chloride sulfation and its effect on deposition in biomass-fired boilers. Energy Fuels 2012;26:6501–8.
- [39] Yongtie C, Kunlin T, Zhimin Z, W Y, Hui W, Guang Z, Li Z, Boon SK, Subbaiah P. Modeling of ash formation and deposition processes in coal and biomass fired boilers: A comprehensive review. Appl Energy 2018;230:1447–544.
- [40] Fatehi H, Costa M, Bai X-S. Numerical study on K/S/Cl release during devolatilization of pulverized biomass at high temperature. Proc Combust Inst 2021;38:3909–17.
- [41] Fatehi H, Weng W, Li Z, Bai X-S, Alden M. Recent development in numerical simulations and experimental studies of biomass thermochemical conversion. Energy Fuels 2021;35:6940–63.
- [42] Hu Z, Wang X, Tan H, Zhou Y. A coupling study of potassium sulfation chemistry and aerosol dynamics for a KCl/SO₂/O₂/H₂O system. Energy Fuels 2020;34:12951–9.
- [43] Chanpirak A, Hashemi H, Frandsen FJ, Wu H, Glarborg P, Marshall P. The chemical coupling between moist CO oxidation and gas-phase potassium sulfation. Fuel 2023;336:127127.
- [44] Yilmaz A, Hindiyarti L, Jensen AD, Glarborg P, Marshall P. Thermal Dissociation of SO₃ at 1000-1400 K. J Phys Chem A 2006;110:6654–9.
- [45] Chanpirak A, Wu H, Glarborg P, Marshall P. An experimental and chemical kinetic modeling study of the role of potassium in the moist oxidation of CO. Fuel 2023;335:127075.
- [46] Pelucchi M, Frassoldati A, Faravelli T, Ruscic B, Glarborg P. High-temperature chemistry of HCl and Cl₂. Combust Flame 2015;162:2693–704.
- [47] Song Y, Hashemi H, Christensen JM, Zou C, Haynes BS, Marshall P, Glarborg P. An exploratory flow reactor study of H₂S oxidation at 30–100 bar. Int J Chem Kinet 2017;49:37–52.
- [48] Schmid D, Weng W, Li S, Karlström O, Hupa M, Li Z, Glarborg P, Marshall P, Aldén M. Optical in-situ measurements and modeling of post-flame sulfation of NaOH(g) and NaCl(g). Fuel 2023;332:126337.
- [49] Chase MW. NIST-JANAF thermochemical tables, Vol. 9. Washington, DC: American Chemical Society; 1998.
- [50] Gurvich LV, Bergman GA, Gorokhov LN, Iorish VS, Leonidov VY, Yungman VS. Thermodynamic properties of alkali metal hydroxides. Part II. Potassium, rubidium, and cesium hydroxides. J Phys Chem Ref Data 1997;26:1031–110.
- [51] Sorvajarvi T, Viljanen J, Toivonen J, Marshall P, Glarborg P. Rate constant and thermochemistry for K + O₂ + N₂ = KO₂ + N₂. J Phys Chem A 2015;119:3329–36.
- [52] Goumri A, Laakso D, Rocha JDR, Francis E, Marshall P. Investigation of the gas-phase kinetics of the reaction K + SO₂ + Ar. J Phys Chem 1993;97:5295–7.
- [53] Burcat A, Ruscic B. Third millenium ideal gas and condensed phase thermochemical database for combustion (with update from active thermochemical tables). Technical report, Argonne, IL (United States: Argonne National Lab. (ANL); 2005, (and updates).
- [54] Vasiliu M, Li S, Peterson KA, Feller D, Gole JL, Dixon DA. Structures and heats of formation of simple alkali metal compounds: Hydrides, chlorides, fluorides, hydroxides, and oxides for Li, Na, and K. J Phys Chem A 2010;114:4272–81.
- [55] Silver JA, Stanton AC, Zahniser MS, Kolb CE. Gas-phase reaction rate of sodium hydroxide with hydrochloric acid. J Phys Chem 1984;88:3123–9.
- [56] Helmer M, Plane JMC. Experimental and theoretical study of the reaction K + HCl. J Chem Phys 1993;99:7696–702.
- [57] J. W. Ager III, Howard CJ. Gas-phase kinetics of the reactions of NaO with H₂, D₂, H₂O, and D₂O. J Chem Phys 1987;87:921–5.
- [58] Martin JCG, Garraway SA, Plane JMC. Reaction kinetics of meteoric sodium reservoirs in the upper atmosphere. J Phys Chem A 2016;120:1330–46.
- [59] Martín JCG, Seaton C, De Miranda MP, Plane JMC. The reaction between sodium hydroxide and atomic hydrogen in atmospheric and flame chemistry. J Phys Chem A 2017;121:7667–74.

- [60] Helmer M, Plane JMC. A study of the reaction $NaO_2+O\to NaO+O_2-$ Implications for the chemistry of sodium in the upper atmosphere. J Geophys Res Atmos 1993;98:23207–22.
- [61] Curtiss LA, Redfern PC, Raghavachari K. Gaussian-4 theory. J Chem Phys 2007;126.
- [62] Marier P, Dibbst HP. The catalytic conversion of SO₂ to SO₃ by fly ash and the capture of SO₂ and SO₃ by CaO and MgO. Thermochim Acta 1974;8:155–65.
- [63] Graham KA, Sarofim AF. Inorganic aerosols and their role in catalyzing sulfuric acid production in furnaces. J Air Waste Manage Assess 1998;48:106–12.
- [64] Belo LP, Elliott LK, Stanger RJ, Spoerl R, Shah KV, Maier J, Wall TF. High-temperature conversion of SO₂ to SO₃: Homogeneous experiments and catalytic effect of fly ash from air and oxy-fuel firing. Energy Fuels 2014;28:7243–51.